Journal of Materials Chemistry A

Essential Effect of the Electrolyte on the Mechanical and Chemical Degradation of $LiNi_{0.8}Co_{0.15}Al_{0.05}O_2$ Cathodes upon Long-Term Cycling

Journal:	*Journal of Materials Chemistry A*
Manuscript ID	TA-COM-08-2020-007814.R2
Article Type:	Communication
Date Submitted by the Author:	23-Dec-2020
Complete List of Authors:	Liu, Xiaoming; Oak Ridge National Laboratory, CNMS Zhan, Xiaowen; University of Kentucky Hood, Zachary ; Argonne National Laboratory Li, Wangda; University of Texas at Austin, Materials Science and Engineering Donovan, Leonard; Oak Ridge National Laboratory, Manthiram, Arumugam; University of Texas at Austin, Materials Science and Engineering Chi, Miaofang; Oak Ridge National Laboratory, Center for Nanophase Materials Sciences

Article to Journal of Materials Chemistry A, Revision 2, 12/2020

Essential Effect of the Electrolyte on the Mechanical and Chemical Degradation of $LiNi_{0.8}Co_{0.15}Al_{0.05}O_2$ Cathodes upon Long-Term Cycling

Xiaoming Liu,[1,#] Xiaowen Zhan,[1,2,#] Zachary D. Hood,[3,#] Wangda Li,[4] Donovan N. Leonard[5], Arumugam Manthiram,[4] Miaofang Chi[1,*]

[1] Center for Nanophase Materials Sciences, Oak Ridge National Laboratory, Oak Ridge, TN 37831, USA
[2] Department of Chemical and Materials Engineering, University of Kentucky, Lexington, Kentucky 40506, USA
[3] Applied Materials Division, Argonne National Laboratory, Lemont, IL, 60439, USA
[4] Materials Science and Engineering Program and Texas Materials Institute, The University of Texas at Austin, Austin, TX 78712, USA
[5] Materials Science and Technology Division, Oak Ridge National Laboratory, Oak Ridge, TN 37831, USA

[#] Equal contribution
[*] Correspondence to: chim@ornl.gov

Keywords: Crack propagation, EELS, Electron microscopy, Li-ion batteries, Nickel-rich layered oxides, Structural degradation

Abstract

Capacity fading during long-term cycling (>1500×) is still a critical challenge for Li-ion batteries that use Ni-rich layered oxides, *e.g.* $LiNi_{0.8}Co_{0.15}Al_{0.05}O_2$ (NCA), as the cathode. Microcracks have been previously recognized as one of the primary reasons for the observed capacity fade. Although there exists a generally developed mechanical understanding of microcracks, the role of the electrolyte has not been clearly understood, especially after extended cycling and at the atomic scale. Here, we unveil the microstructural evolution of spherical NCA secondary particles after long-term cycling using scanning transmission electron microscopy accompanied with electron energy loss spectroscopy. We found that the microcracks initiated and grew through grain boundaries, which then serve as the pathway for electrolyte penetration into secondary NCA particles. Additionally, the rock-salt phase reconstruction is prone to occur at the (003) surfaces of the primary particles or the crack surfaces, largely due to electrolyte ($LiPF_6$ EC/EMC) corrosion. Crack propagation within the NCA grains is primarily a joint consequence from electrolyte corrosion and mechanical strain during lithiation/delithiation. During extended cycling, due to the distinctive surface facets, the primary grains located in the center of the secondary particles experience more intensive electrolyte corrosion, leading to a reduced contact with nearby particles, impairing the overall capacity. These results establish the initiation and growth mechanism of microcracks and voids in NCA-based cathodes during cycling and point out the role of the electrolyte in affecting the degradation of NCA-based cathodes.

Introduction

The successful implementation of lithium-ion batteries relies on the development of effective electrodes with an overall higher energy density, faster charging, safer operation, lower cost, and longer life, in which all are vital for technologies that require mobile batteries such as hybrid or all-electric vehicles.[1-3] Nickel-based layered oxides have witnessed widespread commercialization due to their high capacity (~ 200 mAh/g until ~4.6 V *vs.* Li/Li^+) and impressive rate performance. $LiNi_{0.8}Co_{0.15}Al_{0.05}O_2$ (NCA) and $LiNi_{1-x-y}Co_xMn_yO_2$ (NCM, 1-x-y≥0.5) are two representative layered oxide materials that attract the most attention. However, NCA exhibits drastic capacity fading with a concomitant rise in impedance with cycling and poor thermal stability.[4] Even though NCM presents a better electrochemical performance, as a substitute material of $LiNiO_2$, Ni-rich layered oxides still suffer from much intrinsic structural instability brought by the high Ni content.[5-11]

Extensive efforts have focused on unveiling the origin of the performance deterioration of these layered oxide cathodes upon cycling. Several degradation mechanisms have been proposed thus far, *e.g.*, irreversible formation of inactive and highly resistive Ni^{2+}/Ni^{3+} species like NiO,[12-13] oxidation of electrolyte components,[14] and dissolution of the transition metals induced by HF.[15] Based on these findings, multiple strategies have been investigated including surface coatings[16-18] and bulk doping[19-20] to stabilize the cathode materials. In addition to the aforementioned chemical instability, mechanical failure originating from microcrack generation is another issue causing degradation. In both NCA and NCM oxides, cracking has been mainly associated with anisotropic lattice changes of materials during extraction and insertion of lithium ions, leading to a separation and finally an isolation of primary particles.[9, 13, 22-27] Such intergranular cracks not only compromise electrical contact which results in loss of active materials, but also accelerate cathode/electrolyte side reactions.[24] Besides, intragranular cracks were also reported in primary particles of NCM electrode. It was suggested that the high cut-off voltage (between 4.5 V and 4.7 V *vs.* Li/Li^+) is the direct driving force for intragranular crack generation where dislocations act as a nucleation site for microcrack incubation.[28] Importantly, these cracks expose the fresh surface in primary particles to the electrolyte, which gradually degrades the battery performance.[28-29] Recently, the intrinsic origin of both types of cracks in $LiNi_{0.8}Co_{0.1}Mn_{0.1}O_2$ were also revealed theoretically using multiscale modeling.[23, 29] Despite these in-depth theoretical studies, an atomistic insight is lacking for the NCA-based cathode materials after long-term cycling in

practical full cells, which is a prerequisite for continuous efforts in determining the relationship between *i)* mechanics, *ii)* structure, and *iii)* electrochemistry during the cathode degradation.

Our previous work[30] compared the long-term cycling performance of NCA and NCM cathode materials in high-voltage graphite full cells. We found that NCA, in contrast to NCM, suffered from more secondary particle pulverization after 1500 cycles despite its slightly higher capacity retention. Instead of intragranular cracks, which prevail at higher delithiation states, only intergranular cracks were observed since the cut-off voltage was set at 4.4 V *vs.* graphite (~4.5 V *vs.* Li/Li^+).[28] Thus, it is critical to expose the origin of intergranular cracks formation with the associated structural evolution especially after long-term cycling. Still, unveiling the origin of intergranular cracks request techniques with superb spatial resolution.

Advanced scanning transmission electron microscopy (STEM) combined with electron energy loss spectroscopy (EELS) provide chemical and structural information at a necessary high spatial resolution and energy resolution. The local structure and chemical evolution can be clearly identified, however, was hardly achievable by previously applied characterization techniques like X-ray absorption spectroscopy[31-32] and X-ray diffraction.[24] Taking advantage of electron microscopy, the structural changes near grain boundaries of NCA secondary particles were previously explored by Zheng *et al*., while the evolution of the surface crystallographic and electronic structure of NCA particles with depth of charge was examined by Hwang *et al*.[33] Nevertheless, both works primarily focused on the first cycle of NCA in a half cell configuration. It is well known that the adverse effects of microstructural evolution (*e.g.,* microcrack generation) on cell performance tend to become dominant only during long-term electrochemical operation.[24, 30] Although it has been shown that the electrolyte penetrates all the way into the interior of secondary particles even in the initial cycle,[21] the mechanical degradation of NCA electrodes has been predominantly linked to anisotropic strain changes.[9, 13, 21-24] Less attention has been paid to the essential effect of electrolyte.[34] Herein, we combine scanning electron microscopy/focused ion beam (SEM/FIB), STEM, and EELS to analyze the NCA-based cathode before and after 1500 cycles in a full cell with graphite as the anode and Lithium hexafluorophosphate in ethylene carbonate and dimethyl carbonate ($LiPF_6$ EC/DMC) as the electrolyte. Detailed information regarding chemical and structural evolutions at the atomic scale demonstrates the relationships among mechanical degradations, electrolyte-induced corrosion, and inner structural characteristics of NCA particles.

Experimental Methods

The sample preparation and electrochemical testing details of $LiNi_{0.8}Co_{0.15}Al_{0.05}O_2$ (NCA) materials are described elsewhere.[30] NCA electrode was harvested from pouch-type graphite full cell after 1500 cycles at 25 °C under C/5 rate using a high cut-off voltage of 4.4 V. The cathode electrode was infused with electrolyte of 1 M $LiPF_6$ in ethylene carbonate-ethyl methyl carbonate (EC:EMC, 3:7 by weight) with 2 wt% vinylene carbonate. TEM specimen was then prepared by FIB lift out using a FEI Nova 200 dual beam microscopy. The STEM/EELS study was conducted on an aberration-corrected FEI Titan S 8-300 TEM/STEM equipped with a Gatan Image Filter Quantum-865 operated at 300 kV. HAADF-STEM imaging was collected with a probe convergence angle of 30 mrad and a large inner collection angle of 65 mrad. EELS analysis was carried out in STEM mode using dual EELS mode with a 5 mm aperture with a spectrometer collection angle of 40 mrad and a dispersion of 0.3 eV/channel. Energy shift of each EELS spectrum was calibrated by using its simultaneously acquired zero-loss spectrum. FIB slice and view tomography was performed on a Helios Hydra UX DualBeam using Xe^+ Plasma FIB (PFIB) at Thermo Fisher Scientific Inc. , which allows high throughput milling for large volume characterization, with minimized contamination of the sample. It's noted that more than 50 regions on multiple particles and specimens were studied to show similar phenomena. Representative results are presented in this manuscript.

Results and Discussion

Cathode-dominated capacity fading of full-cells

To obtain samples for post-mortem microstructure examination, NCA electrodes were dissembled from pouch-type graphite full cells after long-term cycling at 25 °C with a C/5 charge-discharge rate. Detailed and comprehensive analyses on the electrochemical performances of the same samples have been discussed in our previous work.[30] Here, we are primarily focusing on the microstructural evolution for the NCA particles before and after the 1500 cycles. As we previously reported[30], with the initial capacity of 191 mAh/g at C/10 (1 of the 5 formation cycles), the

retention of the 1500-cycle discharge capacity is 80% for the NCA electrode. During cycling, the NCA electrode shows a continuous capacity fade and an increase in the voltage polarization, as the data we previously published.[30] Similar behaviors can be observed in reference half-cell testing of NCA electrode harvested from pouch full cells before and after long-term cycling which implies the capacity loss and voltage decline mainly originate from the cathode. This insight is also supported by electrochemical impedance spectroscopy (EIS) results, where the full-cell impedance is predominantly contributed by the cathode side. Obviously, NCA suffers from more particle cracking and pulverization than Ni-rich NCM cycled with a broad Li content range (2.5–4.4 V *vs.* carbon) after 1500 cycles.[30] Therefore, we conducted further investigations in this work on the microstructural degradations of NCA.

Microstructure of pristine $LiNi_{0.8}Co_{0.15}Al_{0.05}O_2$

Figure 1 shows the high-angle annular dark-field HAADF-STEM images and EELS spectra of the pristine NCA material. A transition-metal co-precipitation method is used to prepare micrometer-sized secondary NCA particles comprised of 100-200 nm primary particles as shown in Figure 1a. Such a "meatball" design not only decreases the lithium diffusion distance (small primary particles) but increases the tap density (uniform secondary-particle size distribution), which together enable an excellent electrochemical performance.[35] The layered structure, with a $R\bar{3}m$ space group, is clearly seen in a representative primary particle accompanied with a fast Fourier transform (FFT) pattern (Figure 1b). The bright and dark spots belong to the slabs of transition metal (TM) ions and Li ions parallel to the (003) plane, respectively. It is noted that the Li ions are much lighter than TM ions such that contributes less to the HAADF contrast. Figure 1c shows a representative grain boundary (GB), which is located at the dark region, between two primary particles. EELS spectra acquired at the bulk and GB are compared in Figure 1d-f. No obvious difference was observed, as the Ni/Co-*L* edge and O-*K* edges match well with the reported electronic structures of layered NCA, [30, 33] suggesting a uniform distribution of the crystallographic and chemical structures throughout the pristine secondary particles. It should be noted that the pristine NCA particles synthesized at 800 °C is not perfectly dense and there exist loosely contacted primary grains as shown in Figure S1. Most likely, it is the preference position for the generation of grain separations during early charging/discharging processes, possibly providing preferred paths for the electrolyte.

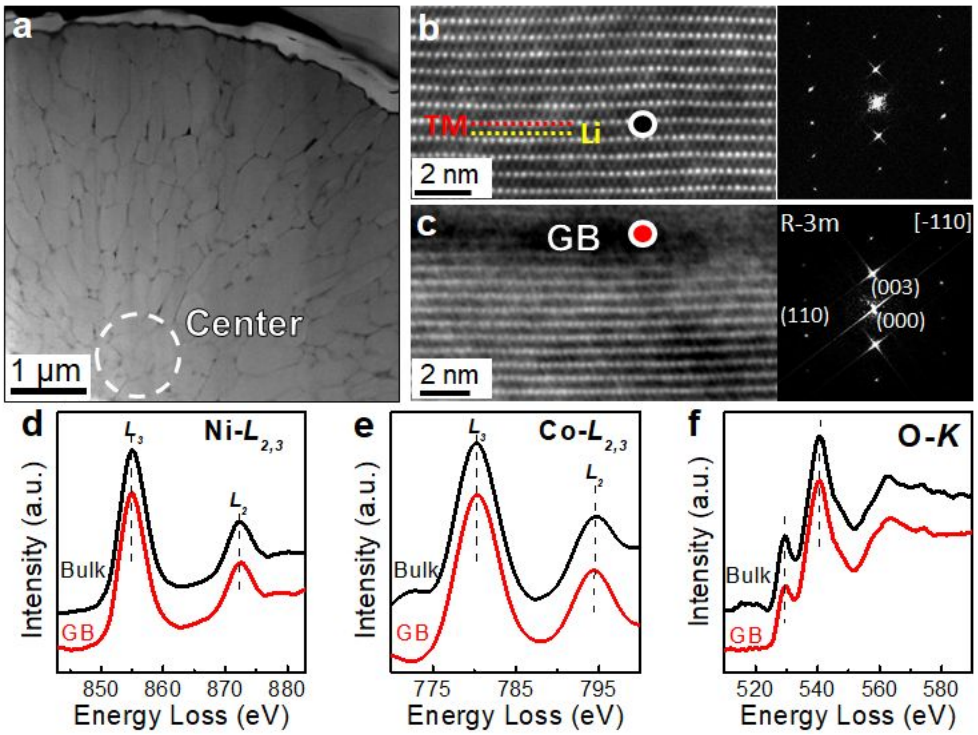

Figure 1. HAADF-STEM images and EELS spectra of the pristine NCA cathode. (a) Cross-section of a secondary particle. (b-c) High-resolution STEM images and FFT patterns of NCA at the bulk and a representative grain boundary. (d-f) EELS spectra measured at the points indicated in panel b and c.

Electrolyte-controlled structural degradations near cracks/voids

Figure 2 presents SEM and HAADF-STEM images of the cycled NCA material after 1500 cycles in pouch-type full cells with graphite as the anode. Microcracks along the GBs and the presence of voids primarily in the central part of are revealed within a representative cycled NCA secondary particle (Figure 2a). Supplemental Video 1 shows a series of slice-and-view scanning electron microscopy (SEM) images during FIB slicing of a secondary particle of NCA after 1500 cycles. It is clearly revealed that the voids are primary located in the center of the secondary particle and propagate radially outwards under extended cycles. More images of secondary particles are provided in Figure S2. Interestingly, as shown in Figure 2a, cracks preferentially occur at specific GBs, which were likely between those initially loosely contacted primary grains (Figure S1). These cracks are aligned along the radial direction to form a line from the particle surface to the central voids, which can be related to the transport process of the dissolved cations (*e.g.,* Li^+) in the liquid during battery cycling. This observation is in good agreement with the findings of a recent work

by Yan *et al.*,[34] where it was suggested that intergranular cracks are essentially caused by not only the build-up of lattice microstrain, but also the liquid electrolyte that penetrates into the GBs and dissolves the cathode. Two commonly noted observations can also support the overlooked electrolyte "aggression" towards corroding the cathode and causing intergranular cracks. First, high-density cracks are gradually generated during extended cycling, which is widely reported for NCM and NCA cathodes.[18, 24, 28, 36] In the case of anisotropic strain being the sole cause for the propagation of cracks, one would expect many cracks in the initial cycles. To mitigate this issue, outer surface coatings, such as Li_3PO_4,[34] were used to modify the cathode secondary particles without modifying the GBs; collectively, this strategy partially blocks the electrolyte penetration into the cathode and suppresses the dissolution/structural degradation process.[24] Still, not much is known with regards to *i)* the connection between electrolyte penetration and dissolution/structural degradation in NCA and *ii)* the atomic configuration of microcracks after extended cycling.

The relationship between electrolyte penetration and intergranular cracking was evidenced by the structural degradations at different GBs and central voids. Figure 2b shows an STEM image of a typical GB at the crack line, which is highlighted in Figure 2a. Below the microcrack (dark contrast), there is a white surface layer of about 2 nm in thickness which possesses obvious structural differences when compared to the bulk region (layered structure). Such a surface reconstruction is due to the transformation of the original $R\bar{3}m$ layered structure into a NiO-type $Fm\bar{3}m$ rock-salt phase.[9-10, 30, 33] It is noted that these results specifically highlight the microcracks at GBs where the electrolyte penetrated deep into the cracks. Even intact GBs, beyond the crack line, suffered from some extent of reconstruction, see Figure 2c. Here, the extent of surface reconstruction is significantly diminished (*e.g.* no obvious rock-salt phase is present) when compared to the microcracks presented in Figure 2b. However, the reconstruction from the ordered layer structure (Figure 2b) to the partially ordered structure (Figure 2c) with extra TM ions at the Li sites is still evident when comparing the grain interior and the GB. Thus, these results could serve as prime evidence for electrolyte penetration through compact GBs. The chemical state evolution at the surfaces close to GBs of the primary particle was examined by EELS. The spectra were acquired at different points, as indicated in Figure 2c. The spectra for the reconstruction layer (A, red) and the bulk (C, blue) were selected to illustrate the trend. The shift of the Ni-$L_{2,3}$ edge towards a lower energy loss indicates the partial reduction of Ni^{3+} (Figure 2d).[36] The increased $I(L_3)/I(L_2)$ ratio (point C: 1.42; point A: 1.81) from the bulk to the reconstructed layer additionally

indicates the change in the oxidation state of Ni between the grain interior and the GB. Cobalt, on the other hand, is more stable than Ni as no obvious energy shift in Co-$L_{2,3}$ edges was observed, as shown in Figure 2e.[32-33, 37] The O-*K* pre-edge peak near 530 eV is ascribed to the transition of electrons from the O 1*s* state to the 2*p* states hybridized with the 3*d* states in TMs (mostly Ni here).[38] The disappearance of this pre-edge in the reconstruction layer (point A) agrees with the occurrence of Ni reduction.[20, 39] It has been suggested that electrolyte can penetrate towards the interior of NCA secondary particles instead of contacting just the periphery of the particle, which is responsible for not only high Li^+ mobility but also a corresponding increase in capacity in the initial cycles.[21, 34] This performance readily explains the observed local structural reconstruction at intact GBs, which are still accessible to liquid electrolytes. Consequently, inactive phases, such as NiO, are generated especially during charging due to side reactions between highly reactive Ni^{4+} species and the electrolyte.[17, 39]

It is also noted that the oxygen K-edge has an obvious change with pre-peak intensity from the bulk of the particle to the surface the grain after long-term cycles. After the normalization of both surface and bulk spectra to their total intensity, an integration of the O-*K* edge between 520 and 570 eV is calculated which shows an 8% intensity decrease at the surface compared to bulk (see Figure S3), indicating a reducing oxygen concentration at surface and suggesting the occurrence of oxygen evolution. It has been reported that oxygen release occurs at the surface of the Ni-rich oxide cathode accompanied by irreversible phase transformation, layered structure to rock salt. Several mechanisms have been proposed to explain the oxygen evolution process, notably: *1)* an overpotential results in activation energy for oxygen 2p band and the formation of O-O bonds that evolves as O_2 gas, and *2)* a local increase in the temperature triggers the transition metal migration that breaks TM-O bonds and favors the O-O reformation.[40-41] The increase of the Ni content in the oxide cathode facilitates oxygen release, as well as the extent of delithiation.

In addition to the surface reconstruction, earlier studies have also connected the structural degradation partly to slow dissolution of the TM ions at the particle surface resulting from HF attack.[42-43] Previous X-ray photoelectron spectroscopy (XPS) and time-of-flight secondary-ion mass spectrometry (TOF-SIMS) mapping analyses have clearly shown the transmission metal species on the graphite anode after long-term cycling.[30] Figure 2g estimated the variation of Ni concentration from the bulk to the GB based on the EELS spectra. For NCA cathode materials, the leaching of Ni ions from the particle was reported to be much more pronounced than that of Co,[17]

which is consistent with the superior stability of Co^{3+} in the layered structure mentioned above. Therefore, negligible Co dissolution is considered. The decreasing trend in Ni content from point C to A (bulk to GB) can serve as additional evidence of electrolyte aggression towards TM dissolution. It is believed that structural degradations can develop internal stresses large enough to initiate or aggravate intergranular cracks in NCA.[17, 24]

HAADF-STEM images and EELS spectra acquired at regions near a central void are also provided in Figure S4, where similar but more dramatic structural evolutions (compared with that near cracks) can be observed. The rock-salt phase layer reaches up to 20 nm thick near the void (Figure S4b-d), and even Co^{3+} show signs of reduction as demonstrated in Figures S4f. The surrounding voids cut the number of electron pathways to the primary particles in the center (away from the binder/carbon medium) which initially relied on GBs for electron transport. As a result, these central particles gradually become electronically isolated and thus electrochemically inactive despite the enhanced accessibility to lithium ions due to electrolyte penetration.[21, 44] In turn, the primary NCA particles have an increased contact area with the electrolyte. Further dissolution and reconstruction at the surface, thereby, will enlarge the separation between the particles and eventually result in completely isolated "dead" particles. Taken collectively, the electrolyte penetration accounts for the observed local surface reconstruction at GBs or near voids. Combined with direct metal dissolution, it can initiate/enlarge particle disintegration apart from the effect of intrinsic anisotropic strain changes. These cracks and voids can lead to excessive formation of cathode-electrolyte interphase and damage the electrical conduction network. In addition, potential oxygen release at the surface of the primary particle may facilitate the cracking of the secondary particles.

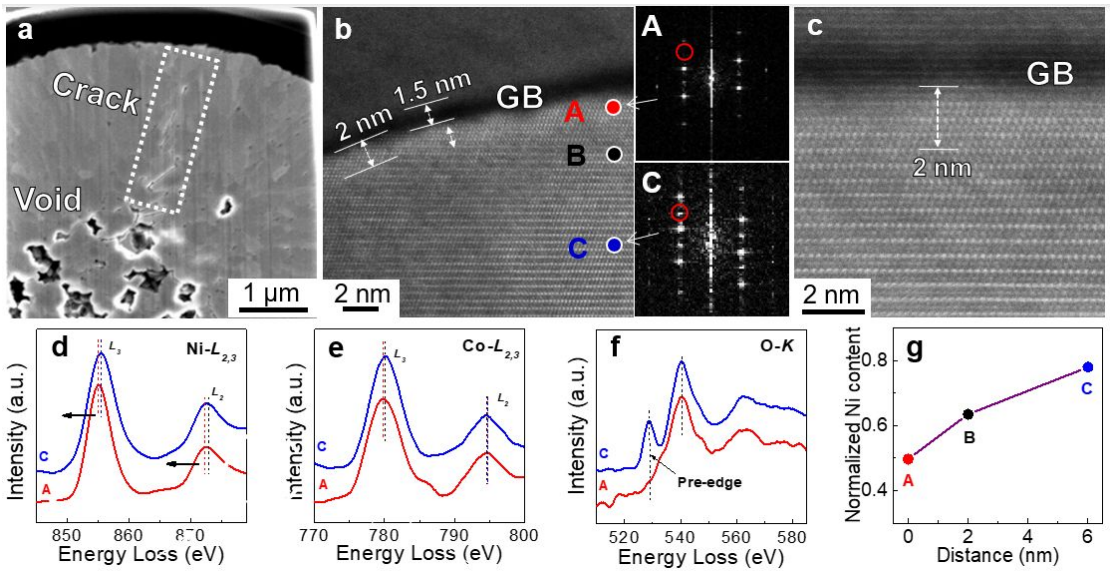

Figure 2. SEM (a) and HAADF-STEM images (b-c) of NCA after 1500 cycles. (a) Cross-section image of a secondary particle. Two representative GBs (b) at and beyond (c) the microcrack line indicated in panel (a). EELS spectra of Ni *L*-edge (d), Co *L*-edge (e), and O *K*-edge (f) acquired at the points indicated in panel (b). (g) Normalized Ni concentration (relative to Co) from the GB to the bulk derived from EELS spectra.

Formation mechanisms for radial cracks and central voids

The microstructural evolution, in the form of cracks and voids, is largely associated with the observed capacity fade in NCA particles after long-term cycling. Nevertheless, the corresponding formation mechanisms remain to be explored and elucidated. Here, we propose that the appearance of radial cracks and central voids are intrinsically related to the spatial distribution of the orientation of the primary particles.

As previously shown in Figure 1, along the radial directions of a NCA secondary particle, the outer grains are typically elongated. In sharp contrast, the central grains are obviously suppressed. A representative region with a void of the cycled secondary particle is shown in Figure 3. High-resolution STEM images (Figure 3b-c) reveal that the radial direction is generally parallel to the *a*-direction, which is perpendicular to the [003] direction of lithium ion intercalation. On one hand, for distorted HCP structure with $c/a > 1.633$ (*e.g.*, NCA), the bonding among atoms within a layer is stronger than that between layers.[45] Therefore, from the perspective of electrolyte aggression, corrosion of the (120) facet is expected to be easier when compared to the (003) facet. Thus, the rock-salt phase forms at the surface through the TM cations inward diffusion along

lithium channels. This result is further supported by the observation in Figure 3b-c, where the (120) facets exhibit a surface reconstruction layer extending more than 10 nm to the particle bulk. In contrast, the GB (on the top) parallel to the (003) facet maintains the original layered structure. It is noted that the contrast of (003) surface is brighter than the (003) grain boundary in Fig. 3b, which could be contributed by both surface reconstruction and the fact that the electron probe is focused on GB region but off on the surface region. Fig. 3c reveals the structure of (003) surface more clearly, which show that the layered structure is remained with a slightly brighter contrast in the three outmost surface Li layers, indicating a partial occupancy of TM ions at the Li sites. On the other hand, it should be noted that the expansion of the void along the [120] direction is also facilitated by anisotropic volume change. During charging, the layered structure mainly expands along the *c* axis and contracts along *a*/*b* axes. A recent computational study on NCM811 suggested that separation typically occurs on the interfaces between contracted primary NCM particles.[23] In regard to both electrolyte-induced corrosion and strain within the particles, intergrain separations (cracks and voids) are expected to initiate and proceed at radial GBs especially between those loosely packed grains in pristine state (Figure S1).

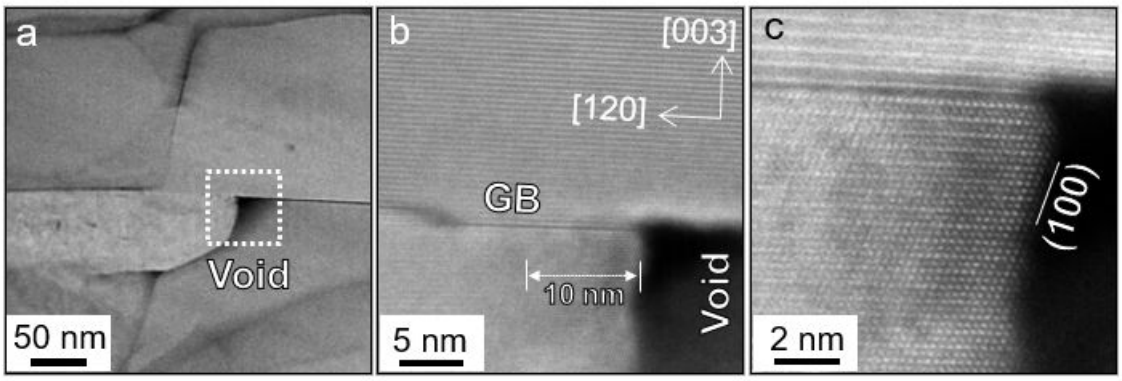

Figure 3. (a) HAADF-STEM images of a typical void in the center of a secondary particle after cycling. (b) Atomic resolution STEM image of the primary particle at the void. (c) A magnified STEM image showing the reconstructed surface phase.

It is generally accepted that the central primary grains are prone to lose electronic contact with surrounding primary particles upon the propagation of intergranular cracks.[21, 44] One possible scenario is that these grains may suddenly become electrochemically inactive, *e.g.*, at the charged

state, as a result of lattice contraction along the tangential direction as illustrated in Figure 4. Unlike peripheral grains that generally recover physical contacts with neighboring grains during the next discharge, these inactive central grains will remain isolated. Consequently, the initial separation will be widened by continuous electrolyte-induced corrosion (*e.g.*, TM dissolution and side reactions between instable Ni^{4+} and the electrolyte). Ultimately, large voids eventually form in the cathode after extended cycling, leading to capacity loss.

Based on the microstructural observations of NCA materials before and after long-term full-cell cycling, we summarize some interesting findings as follows. (1) In cycled secondary particles, major cracks form along certain radial GBs, which are connected with large voids in the center, implying intergranular cracking is initiated through GBs. (2) The primary particles near central voids experience a significantly thicker surface reconstruction layer (with clear evidence of Ni reduction and layered-to-rock salt phase transformation) than the surface of NCA near cracks. Additionally, minor surface reconstruction was revealed near GBs which are free of cracks, suggesting that the electrolyte could penetrate throughout a secondary particle. (3) The primary grains were observed to grow with (003) plane parallel to the radial direction of the secondary particle, along which lithium insertion/extraction occurs. Lattice contraction upon delithiation along the *a*-axis results in separation of grains and more surface contact with electrolyte, which in turn facilitates electrolyte-induced corrosion along the *ab* facet. (4) The large inner voids within secondary particles essentially arise from the limited electronic path to the central part of primary particles. Once excluded from the conduction network, these inactive grains with existing unrecoverable intergrain separation will gradually develop voids due to electrolyte-assisted dissolution and side reactions between the NCA cathode and the electrolyte.

Following these findings, possible strategies can alleviate the abovementioned degradation in NCA cathodes. First, engineering the GBs could effectively block electrolyte penetration while maintaining sufficient electronic and ionic pathways to individual primary particles. For instance, Kim *et al*. improved the performance of NCA via a $LiCoO_2$-containing glue-nanofiller that can protect the surface of primary particles and narrow the intergrain gaps.[36] Although the improved grain-to-grain contact helps the interfacial electron transport via $LiCoO_2$, the low Li-ion conductivity of $LiCoO_2$ might restrict the accessibility of inner primary particles to lithium ions. One may argue that the electrolyte can penetrate all the way to the interior of secondary particles.[21, 28] However, this penetration may be questionable, especially since such

interfacial coatings may limit the penetration to large GBs. On the other hand, Yan *et al*. designed a solid electrolyte coating of Li_3PO_4 that can be infused along GBs within Ni-rich NCM secondary particles. The infused layer was suggested to simultaneously stabilize the surface while providing fast Li-ion transport, thereby achieving a significant improvement in the cycling stability.[34] Nonetheless, this may not solve the poor electronic connection suffered by central primary particles. Thus, we suggest that new coating agents with mixed ionic/electronic conductivity to be explore for advanced cathode materials in batteries. Another possible approach lies in reducing the generation of radial cracks by tuning the intrinsic structural features such as the grain-orientation of the primary particles. Recent work by Yang *et al.* demonstrated that the grain-orientation characteristics of NCM622 can be successfully inherited from $Ni_{0.6}Co_{0.2}Mn_{0.2}(OH)_2$ precursors.[46] More importantly, exposure of more (100) or (010) to lithium insertion/extraction was found to favor fast lithium diffusion and a low cation mixing.[46] This performance potentially constitutes a tradeoff between the fast Li-ion transport and less particle disintegration (from electrolyte-induced corrosion and mechanical contraction). Future efforts in addressing this issue may open new opportunities to decipher better structural designs of cathode materials.

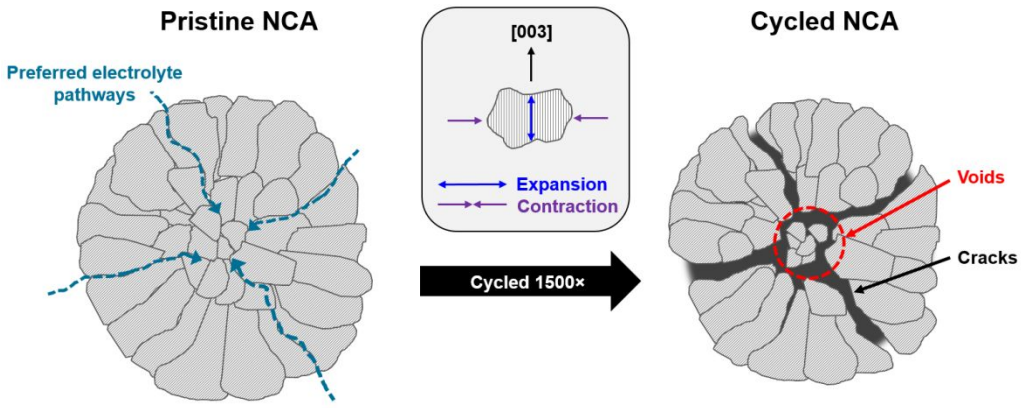

Figure 4. Schematic illustration of forming aligned cracks and central voids in NCA particles after long-term cycling.

Conclusions

In conclusion, the formation mechanism of microcracks and large voids within the secondary particle of NCA cathode was systematically investigated through electron microscopy

and EELS analysis. After charging/discharging for 1500 cycles of practical full-cells, the microcrack was found to initiate and grow along GBs, all the way from the surface to the interior of the NCA secondary particles. Such intergranular cracks ultimately become connected and induce the formation of large central voids. Despite the well accepted mechanical aspect, in this work, it is suggested that the overlooked electrolyte impact is another non-negligible reason causing the microstructure evolution, which results in battery degradation upon long-term cycling. It is evident that not only the surface at the microcracks, namely the separated GBs, but also the intact GBs, to some extent, experience structural reconstruction by electrolyte-induced corrosion. Accordingly, GBs are the pathway of electrolyte penetration into the NCA secondary particle. In turn, the electrolyte facilitates the microcrack initiation and growth during repeated extraction/expansion of the primary particles upon cycling. We also discovered that the rock-salt phase forms thicker along (003) planes, through the lithiation/delithiation channels, compared to that of the perpendicular direction. This result indicates that the facets parallel to the [003] direction are vulnerable to the electrolyte. Considering the irregular geometry of primary particles, mechanical strain, as well as electrolyte-induced corrosion are expected to cause loss of electronic and ionic contact, especially in the interior of secondary particles. At certain stages, the primary particles cannot recover after charging. Thereby, the cracks grow and ultimately isolate the primary particles, resulting in large voids. Our work has unveiled the overlooked impact of the electrolyte on the formation of microcracks and voids. The insight from this work will serve as guidance to mitigate microcrack generation and improve the long-term cycling performance of next-generation Li-ion batteries.

Conflicts of interest

The authors have no conflicts of interest to declare.

Acknowledgements

This research was sponsored by the Center for Nanophase Materials Sciences at Oak Ridge National Laboratory. X. L. was supported by the Basic Energy Sciences (BES), Materials Sciences and Engineering Division, Office of Science, U.S. Department of Energy (DOE). Part of the data

analysis was supported by DOE office of science early career research program ERKCZ55 – KC040304 (M. C.). W. L and A.M. would like to thank the support from the Assistant Secretary for Energy Efficiency and Renewable Energy, Office of Vehicle Technologies of the U.S. Department of Energy through the Advanced Battery Materials Research (BMR) Program (Battery500 Consortium) award number DE-EE0007762. Argonne National Laboratory's contribution (Z.D.H.) is based upon work supported by Laboratory-Directed Research and Development (LDRD) funding from Argonne National Laboratory, provided by the Director, Office of Science, of the U.S. Department of Energy under Contract No. DE-AC02-06CH11357. Authors would like to thank Dr. Ron Kelley and Dr. Lane Wooten at Thermo Fisher Scientific Nanoport demonstration facility for the FIB-SEM tomography work.

References:

1. Tarascon, J.-M.; Armand, M., Issues and challenges facing rechargeable lithium batteries. In *Materials For Sustainable Energy: A Collection of Peer-Reviewed Research and Review Articles from Nature Publishing Group*, World Scientific: 2011; pp 171-179.
2. Thackeray, M. M.; Wolverton, C.; Isaacs, E. D., Electrical energy storage for transportation—approaching the limits of, and going beyond, lithium-ion batteries. *Energy & Environmental Science* **2012,** *5* (7), 7854-7863.
3. Lin, Z.; Liu, T.; Ai, X.; Liang, C., Aligning academia and industry for unified battery performance metrics. *Nature communications* **2018,** *9* (1), 1-5.
4. Whittingham, M. S., Lithium batteries and cathode materials. *Chemical reviews* **2004,** *104* (10), 4271-4302.
5. Zheng, J.; Kan, W. H.; Manthiram, A., Role of Mn Content on the Electrochemical Properties of Nickel-Rich Layered LiNi0. 8–x Co0. 1Mn0. 1+ x O2 (0.0≤ x≤ 0.08) Cathodes for Lithium-Ion Batteries. *ACS applied materials & interfaces* **2015,** *7* (12), 6926-6934.
6. Sun, H.-H.; Choi, W.; Lee, J. K.; Oh, I.-H.; Jung, H.-G., Control of electrochemical properties of nickel-rich layered cathode materials for lithium ion batteries by variation of the manganese to cobalt ratio. *Journal of Power Sources* **2015,** *275*, 877-883.
7. Xiong, X.; Wang, Z.; Yan, G.; Guo, H.; Li, X., Role of V2O5 coating on LiNiO2-based materials for lithium ion battery. *Journal of Power Sources* **2014,** *245*, 183-193.
8. Kim, N. Y.; Yim, T.; Song, J. H.; Yu, J.-S.; Lee, Z., Microstructural study on degradation mechanism of layered LiNi0. 6Co0. 2Mn0. 2O2 cathode materials by analytical transmission electron microscopy. *Journal of power sources* **2016,** *307*, 641-648.
9. Mu, L.; Lin, R.; Xu, R.; Han, L.; Xia, S.; Sokaras, D.; Steiner, J. D.; Weng, T.-C.; Nordlund, D.; Doeff, M. M., Oxygen release induced chemomechanical breakdown of layered cathode materials. *Nano letters* **2018,** *18* (5), 3241-3249.

10. Lin, F.; Markus, I. M.; Nordlund, D.; Weng, T.-C.; Asta, M. D.; Xin, H. L.; Doeff, M. M., Surface reconstruction and chemical evolution of stoichiometric layered cathode materials for lithium-ion batteries. *Nature communications* **2014,** *5* (1), 1-9.
11. Xia, J.; Ma, L.; Nelson, K.; Nie, M.; Lu, Z.; Dahn, J., A study of Li-ion cells operated to 4.5 V and at 55° C. *Journal of The Electrochemical Society* **2016,** *163* (10), A2399.
12. Muto, S.; Sasano, Y.; Tatsumi, K.; Sasaki, T.; Horibuchi, K.; Takeuchi, Y.; Ukyo, Y., Capacity-fading mechanisms of LiNiO2-based lithium-ion batteries: II. diagnostic analysis by electron microscopy and spectroscopy. *Journal of the electrochemical society* **2009,** *156* (5), A371.
13. Sasaki, T.; Godbole, V.; Takeuchi, Y.; Ukyo, Y.; Novák, P., Morphological and structural changes of Mg-substituted Li (Ni, Co, Al) O2 during overcharge reaction. *Journal of The Electrochemical Society* **2011,** *158* (11), A1214.
14. Cherkashinin, G.; Motzko, M.; Schulz, N.; Späth, T.; Jaegermann, W., Electron spectroscopy study of Li [Ni, Co, Mn] O2/electrolyte interface: electronic structure, interface composition, and device implications. *Chemistry of Materials* **2015,** *27* (8), 2875-2887.
15. Aurbach, D., Review of selected electrode–solution interactions which determine the performance of Li and Li ion batteries. *Journal of Power Sources* **2000,** *89* (2), 206-218.
16. Xu, Y.; Liu, Y.; Lu, Z.; Wang, H.; Sun, D.; Yang, G., The preparation and role of Li2ZrO3 surface coating LiNi0. 5Co0. 2Mn0. 3O2 as cathode for lithium-ion batteries. *Applied Surface Science* **2016,** *361*, 150-156.
17. Lee, S.-H.; Yoon, C. S.; Amine, K.; Sun, Y.-K., Improvement of long-term cycling performance of Li [Ni0. 8Co0. 15Al0. 05] O2 by AlF3 coating. *Journal of Power Sources* **2013,** *234*, 201-207.
18. Kim, H.; Kim, M. G.; Jeong, H. Y.; Nam, H.; Cho, J., A new coating method for alleviating surface degradation of LiNi0. 6Co0. 2Mn0. 2O2 cathode material: nanoscale surface treatment of primary particles. *Nano letters* **2015,** *15* (3), 2111-2119.
19. Schipper, F.; Bouzaglo, H.; Dixit, M.; Erickson, E. M.; Weigel, T.; Talianker, M.; Grinblat, J.; Burstein, L.; Schmidt, M.; Lampert, J., From surface ZrO2 coating to bulk Zr doping by high temperature annealing of nickel-rich lithiated oxides and their enhanced electrochemical performance in lithium ion batteries. *Advanced Energy Materials* **2018,** *8* (4), 1701682.
20. Li, X.; Zhang, K.; Wang, M.; Liu, Y.; Qu, M.; Zhao, W.; Zheng, J., Dual functions of zirconium modification on improving the electrochemical performance of Ni-rich LiNi0.8Co0.1Mn0.1O2. *Sustainable Energy and Fuels* **2018,** *2* (2), 413-421.
21. Miller, D. J.; Proff, C.; Wen, J.; Abraham, D. P.; Bareno, J., Observation of microstructural evolution in Li battery cathode oxide particles by in situ electron microscopy. *Advanced Energy Materials* **2013,** *3* (8), 1098-1103.
22. Lee, E.-J.; Chen, Z.; Noh, H.-J.; Nam, S. C.; Kang, S.; Kim, D. H.; Amine, K.; Sun, Y.-K., Development of microstrain in aged lithium transition metal oxides. *Nano letters* **2014,** *14* (8), 4873-4880.
23. Lim, J.-M.; Hwang, T.; Kim, D.; Park, M.-S.; Cho, K.; Cho, M., Intrinsic origins of crack generation in Ni-rich LiNi 0.8 Co 0.1 Mn 0.1 O 2 layered oxide cathode material. *Scientific reports* **2017,** *7*, 39669.

24. Liu, H.; Wolf, M.; Karki, K.; Yu, Y.-S.; Stach, E. A.; Cabana, J.; Chapman, K. W.; Chupas, P. J., Intergranular Cracking as a Major Cause of Long-Term Capacity Fading of Layered Cathodes. *Nano Letters* **2017,** *17* (6), 3452-3457.
25. Ryu, H.-H.; Park, K.-J.; Yoon, C. S.; Sun, Y.-K., Capacity Fading of Ni-Rich Li [Ni x Co y Mn1−x−y] O2 (0.6≤ x≤ 0.95) Cathodes for High-Energy-Density Lithium-Ion Batteries: Bulk or Surface Degradation? *Chemistry of Materials* **2018,** *30* (3), 1155-1163.
26. Watanabe, S.; Kinoshita, M.; Hosokawa, T.; Morigaki, K.; Nakura, K., Capacity fading of LiAlyNi1− x− yCoxO2 cathode for lithium-ion batteries during accelerated calendar and cycle life tests (effect of depth of discharge in charge–discharge cycling on the suppression of the micro-crack generation of LiAlyNi1− x− yCoxO2 particle). *Journal of Power Sources* **2014,** *260*, 50-56.27.
27. Watanabe, S., Kinoshita, M., Hosokawa, T., Morigaki, K., & Nakura, K. (2014). Capacity fade of LiAlyNi1− x− yCoxO2 cathode for lithium-ion batteries during accelerated calendar and cycle life tests (surface analysis of LiAlyNi1− x− yCoxO2 cathode after cycle tests in restricted depth of discharge ranges). *Journal of Power Sources*, *258*, 210-217.
28. Yan, P.; Zheng, J.; Gu, M.; Xiao, J.; Zhang, J.-G.; Wang, C.-M., Intragranular cracking as a critical barrier for high-voltage usage of layer-structured cathode for lithium-ion batteries. *Nature communications* **2017,** *8* (1), 1-9.
29. Min, K.; Cho, E., Intrinsic origin of intra-granular cracking in Ni-rich layered oxide cathode materials. *Physical Chemistry Chemical Physics* **2018,** *20* (14), 9045-9052.
30. Li, W.; Liu, X.; Celio, H.; Smith, P.; Dolocan, A.; Chi, M.; Manthiram, A., Mn versus Al in Layered Oxide Cathodes in Lithium-Ion Batteries: A Comprehensive Evaluation on Long-Term Cyclability. *Advanced Energy Materials* **2018,** *8* (15).
31. Bak, S.-M.; Nam, K.-W.; Chang, W.; Yu, X.; Hu, E.; Hwang, S.; Stach, E. A.; Kim, K.-B.; Chung, K. Y.; Yang, X.-Q., Correlating Structural Changes and Gas Evolution during the Thermal Decomposition of Charged Li x Ni0. 8Co0. 15Al0. 05O2 Cathode Materials. *Chemistry of Materials* **2013,** *25* (3), 337-351.
32. Yoon, W.-S.; Haas, O.; Muhammad, S.; Kim, H.; Lee, W.; Kim, D.; Fischer, D. A.; Jaye, C.; Yang, X.-Q.; Balasubramanian, M., In situ soft XAS study on nickel-based layered cathode material at elevated temperatures: a novel approach to study thermal stability. *Scientific reports* **2014,** *4*, 6827.
33. Zheng, S.; Huang, R.; Makimura, Y.; Ukyo, Y.; Fisher, C. A.; Hirayama, T.; Ikuhara, Y., Microstructural changes in LiNi0. 8Co0. 15Al0. 05O2 positive electrode material during the first cycle. *Journal of The Electrochemical Society* **2011,** *158* (4), A357.
34. Yan, P.; Zheng, J.; Liu, J.; Wang, B.; Cheng, X.; Zhang, Y.; Sun, X.; Wang, C.; Zhang, J.-G., Tailoring grain boundary structures and chemistry of Ni-rich layered cathodes for enhanced cycle stability of lithium-ion batteries. *Nature energy* **2018,** *3* (7), 600-605.
35. Radin, M. D.; Hy, S.; Sina, M.; Fang, C.; Liu, H.; Vinckeviciute, J.; Zhang, M.; Whittingham, M. S.; Meng, Y. S.; Van der Ven, A., Narrowing the Gap between Theoretical and Practical Capacities in Li-Ion Layered Oxide Cathode Materials. *Advanced Energy Materials* **2017,** *7* (20).
36. Kim, H.; Lee, S.; Cho, H.; Kim, J.; Lee, J.; Park, S.; Joo, S. H.; Kim, S. H.; Cho, Y. G.; Song, H. K., Enhancing Interfacial Bonding between Anisotropically Oriented Grains Using a Glue-Nanofiller for Advanced Li-Ion Battery Cathode. *Advanced materials* **2016,** *28* (23), 4705-4712.

37. Wei, Y.; Zheng, J.; Cui, S.; Song, X.; Su, Y.; Deng, W.; Wu, Z.; Wang, X.; Wang, W.; Rao, M., Kinetics tuning of Li-ion diffusion in layered Li (Ni x Mn y Co z) O2. *Journal of the American Chemical Society* **2015,** *137* (26), 8364-8367.
38. Hwang, S.; Chang, W.; Kim, S. M.; Su, D.; Kim, D. H.; Lee, J. Y.; Chung, K. Y.; Stach, E. A., Investigation of changes in the surface structure of LixNi 0.8Co0.15Al0.05O2 cathode materials induced by the initial charge. *Chemistry of Materials* **2014,** *26* (2), 1084-1092.
39. Abraham, D.; Twesten, R.; Balasubramanian, M.; Petrov, I.; McBreen, J.; Amine, K., Surface changes on LiNi0. 8Co0. 2O2 particles during testing of high-power lithium-ion cells. *Electrochemistry communications* **2002,** *4* (8), 620-625.
40. Sharifi-Asl, S.; Lu, J.; Amine, K.; Shahbazian-Yassar, R., Oxygen Release Degradation in Li-Ion Battery Cathode Materials: Mechanisms and Mitigating Approaches. *Advanced Energy Materials* **2019,** *9*, 1900551.
41. Yan, P.; Zheng, J.; Chen, T.; Luo, L.; Jiang, Y.; Wang, K.; Sui, M.; Zhang, J.-G.; Zhang, S.; Wang, C., Coupling of electrochemically triggered thermal and mechanical effects to aggravate failure in a layered cathode. *Nature communications* **2018,** *9* (1), 1-8.
42. Amatucci, G.; Tarascon, J.; Klein, L., Cobalt dissolution in LiCoO2-based non-aqueous rechargeable batteries. *Solid State Ionics* **1996,** *83* (1-2), 167-173.
43. Woo, S.-U.; Yoon, C. S.; Amine, K.; Belharouak, I.; Sun, Y.-K., Significant improvement of electrochemical performance of AlF3-coated Li [Ni0. 8Co0. 1Mn0. 1] O2 cathode materials. *Journal of the Electrochemical Society* **2007,** *154* (11), A1005.
44. Kerlau, M.; Marcinek, M.; Srinivasan, V.; Kostecki, R. M., Reprint of "Studies of local degradation phenomena in composite cathodes for lithium-ion batteries". *Electrochimica Acta* **2007,** *53* (3), 1385-1392.
45. Rao, C. N. R.; Gopalakrishnan, J., *New directions in solid state chemistry*. Cambridge University Press: 1997.
46. Yang, C.-K.; Qi, L.-Y.; Zuo, Z.; Wang, R.-N.; Ye, M.; Lu, J.; Zhou, H.-H., Insights into the inner structure of high-nickel agglomerate as high-performance lithium-ion cathodes. *Journal of Power Sources* **2016,** *331*, 487-494.